Single-Step Rapid Assembly of DNA Origami Nanostructures for Addressable Nanoscale Bioreactors

Yanming Fu,[†,∥] Dongdong Zeng,[†,‡,∥] Jie Chao,[†] Yanqiu Jin,[†] Zhao Zhang,[§] Huajie Liu,*,[†] Di Li,[†] Hongwei Ma,[‡] Qing Huang,[†] Kurt V. Gothelf,[§] and Chunhai Fan*,[†]

[†]Laboratory of Physical Biology, Shanghai Institute of Applied Physics, Chinese Academy of Sciences, Shanghai 201800, China
[‡]Suzhou Institute of Nano-Tech and Nano-Bionics, Chinese Academy of Sciences, 398 Ruoshui Road, Suzhou 215123, China
[§]Centre for DNA Nanotechnology at Department of Chemistry and Interdisciplinary Nanoscience Center (iNANO), Aarhus University, Aarhus 8000, Denmark

S *Supporting Information*

ABSTRACT: Self-assembled DNA origami nanostructures have shown great promise for bottom-up construction of complex objects with nanoscale addressability. Here we show that DNA origami-based 1D nanoribbons and nanotubes are one-pot assembled with controllable sizes and nanoscale addressability with high speed (within only 10−20 min), exhibiting extraordinarily high cooperativity that is often observed in assembly of natural molecular machines in cells (e.g. ribosome). By exploiting the high specificity of DNA-based self-assembly, we can precisely anchor proteins on these DNA origami nanostructures with sub-10 nm resolution and at the single-molecule level. We attach a pair of enzymes (horseradish peroxidase and glucose oxidase) at the inner side of DNA nanotubes and observe high coupling efficiency of enzyme cascade within this confined nanospace. Hence, DNA nanostructures with such unprecedented properties shed new light on the design of nanoscale bioreactors and nanomedicine and provide an artificial system for studying enzyme activities and cascade in highly organized and crowded cell-mimicking environments.
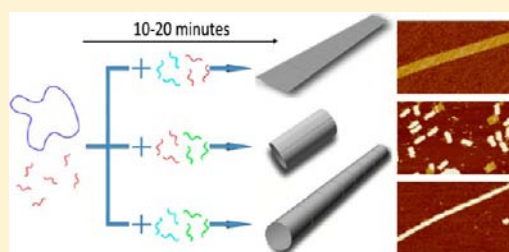
INTRODUCTION

Nanomaterials with controllable geometry and attractive function offer great potential to transform many aspects of electronics, energy, and health of human beings.[1−5] For example, carbon nanotubes (CNTs)[6] and graphene[7−9] have shown great promise for a wide range of applications due to their unique geometry and size-dependent optical/electronic properties. More recently, encapsulation of catalysts in inorganic nanomaterials, e.g., CNTs, has attracted great interest. Such confinement in nanosized matrices results in striking enhancement of catalytic activities, providing new opportunities for high-efficiency nanoreactors.[10,11] However, it remains a great challenge to precisely control the size and morphology of CNTs and other inorganic nanomaterials and to place catalysts (enzymes) in the nanospace in a simple fashion. DNA-based nanomaterials may provide a solution and pave the way to nanoscale bioreactors due to the superior self-assembly ability of DNA molecules.[12,13]

Biomolecules have unparalleled capability to self-assemble into natural "molecular machines" (e.g., a ribosome)[14] *in vivo* with exquisite structure and elaborate function. The emergence of DNA nanotechnology[12] has led to the design and bottom-up construction of a wide range of artificial nanostructures with diverse shapes, geometries, and functions[15−30] as well as nanodevices and nanomachines.[31−35] Particularly, the "DNA origami" strategy developed by Rothemund is a new milestone, which for the first time enables the straightforward production of large size-limited and monodisperse 2D and 3D nanostructures.[15,16,21,26−29,36−38] Extension of the origami technique to assemble individual origami structures into superassemblies is expected to provide micrometer-sized objects with sub-10 nm addressability, such properties are hardly possible to obtain by top-down fabrication.

EXPERIMENTAL SECTION

All short oligo-DNA strands were purchased from Shanghai Sangong Biotech Co. Ltd. M13mp18 viral DNA was purchased from New England Biolabs, Inc. Streptavidin was bought from Amresco, Inc. Heterobifunctional cross-linker N-[(ε-maleimidocaproyloxy) sulfo-succinimide ester] (sulfo-EMCS) was purchased from Pierce. All other chemical reagents and enzymes were purchased from Sinopharm and Sigma-Aldrich and used without further purification.

Short DNA staple strands and the long M13mp18 scaffold strand were mixed in 1× TAE-Mg buffer (40 mM Tris, pH 7.6, 2 mM EDTA, 12.5 mM $MgCl_2$). The final concentrations of the scaffold, each core staple strand, each top/bottom edge staple strand, and each left/right edge staple strand were 3.5, 35, 35, and 17.5 nM, respectively. The DNA origami combinatorial structures were formed with predefined annealing programs using a PTC-200 Peltier Thermal Cycler (MJ Research). Samples of DNA nanostructures were deposited onto a freshly cleaved mica surface and imaged under tapping mode using a J

scanner of a Multimode Nanoscope IIIa AFM (Vecco/Digital Instruments) with a silicon nitride cantilever with sharpened pyramidal tip (OMCL-TR400PSA, Olympus).

DNA−enzyme conjugates were prepared using sulfo-EMCS as a bifunctional cross-linker. In a typical synthesis, glucose oxidase (GOx) or horseradish peroxidase (HRP) (0.5 mL, 12.5 μM in 20 mM phosphate buffer, pH 8.0, containing 0.15 M NaCl) reacted with 100-fold excess of sulfo-EMCS at rt for 6 h. The excess of sulfo-EMCS was removed with a Millipore's 30kD molecule-cutoff Centricon spin-filter. The above product was then mixed with 5-fold excess of thiol-modified DNA at rt for another 6 h. The final DNA−enzyme conjugates were purified with 30kD Centricon spin-filter and characterized with native 10% polyacrylamide gel (PAGE). For preparing enzyme cascade on DNA origami, the DNA−enzyme conjugates were assembled with DNA origami nanostructures (with DNA−enzyme conjugates' complementary strands) in stoichiometric ratio at 37 °C for 30 min. The assembled enzyme cascade on DNA origami (0.25 nM) was then mixed with glucose (0.1 M) and indicator 2′2′-azino-bis[3-ethyl-benzthiazoline-6-sulfonic-acid] (ABTS). The enzyme cascade activity was measured by monitoring absorption value at 418 nm.

■ RESULTS AND DISCUSSION

Design Principle. Previous efforts to construct higher-order DNA origami structures, including linear arrays[8,39,40] and patterns,[37,41−43] typically involve stepwise assembly of size-limited origami pieces and subsequent linkage to form combinatorial nanostructures. Inspired by recent efforts in single-step assembly of some specific higher-order DNA origami nanostructures,[44,45] we herein developed a simple single-step method to produce higher order DNA origami combinatorial structures. The core DNA origami structure is a planar rectangle shape that is composed of a ~7000 base circular single-stranded M13 DNA and 216 short staple strands (Figure 1a).[26] This rectangular nanostructure has a finite size of 100 nm in length and 70 nm in width (Figure 1b). In an attempt to construct complex DNA origami combinatorial structures, we modified the strands on edges of the rectangle to establish connections. As illustrated in Figure 1c, the scaffold strand (M13) and the core staple strands, along with the edge staple strands, were mixed in one-pot for annealing.

Intuitively, these artificial nanostructures have molecular weights that are comparable to ribosomes (~2−3 × 10⁶ Da), the most complex molecular machines in cells, and their assembly involves numerous hybridization events of hundreds of DNA strands (~7000 base pairing), hence such origami folding process was considered to be kinetically slow (usually hours). However, we find that they can in fact be assembled fairly rapidly (usually 10−20 min, see Figures S4−S6 for detailed designs and S15 for rectangular DNA origami results), suggesting high cooperativity during the origami assembly process.

Formation of 1D DNA Nanoribbons. The shape of the obtained nanostructures is critically dependent on the sequences of the edge staple strands. 2D rectangular DNA origami (with staple strands "O$\underline{X}$" and "O$\underline{Y}$") was formed only when the four edges did not contain sticky ends. In contrast, the presence of sticky ends at the top and bottom edges or at the left and right edges led to interedge connections. When sticky ends were placed in extension of the horizontally aligned helices (at the left and right edges of the origami in Figure 1a), adjacent rectangles (using staple strands "M$\underline{X}$", Figures 2a and S2) are assembled in the horizontal direction to form DNA nanoribbons with precisely controlled width (Figure 2b). These nanoribbons have straight linearity with lengths ranging from 0.5 to 2.5 μm. The measured width and height are ~70 and ~2
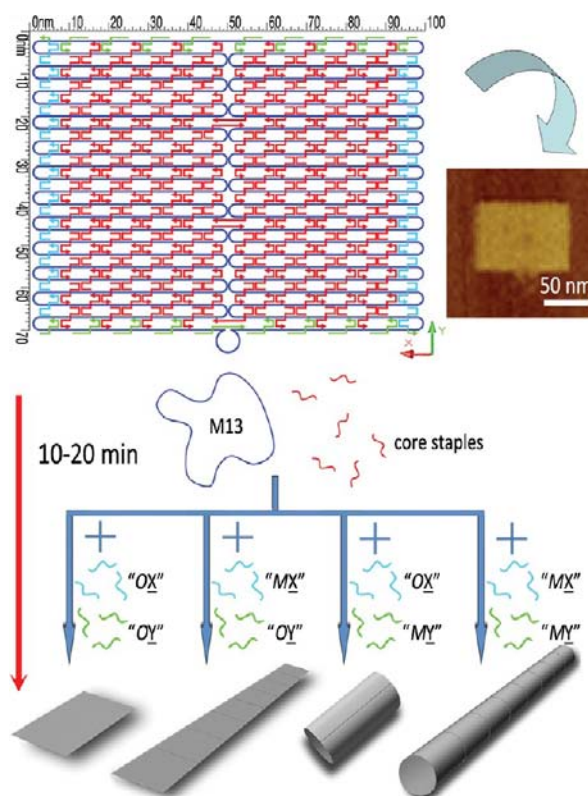

Figure 1. Design principles. (a) Schematic illustration of the rectangular DNA origami. Core staple strands are in red, and edge staple strands are in blue and green. (b) Typical AFM image. (c) One-pot fast construction of DNA origami combinatorial structures. "O" and "M" refer to the staple strands at edges without and with sticky ends, respectively; "$\underline{X}$" means the left and right edges, and "$\underline{Y}$" means the top and bottom edges.

nm, respectively (Figure S16A), consistent with the standard rectangular DNA origami.[26] Importantly, this horizontal assembly is highly efficient, and we observed almost no individual rectangular DNA origami in samples. As a comparison, similar 1D nanoribbons were also prepared using a longer time (2 h) in one-pot assembly (see Figure S17A), which resulted in nanoribbons that were nearly the same as those obtained with a short folding time of 20 min.

Formation of 1D Short DNA Nanotubes. When the sticky ends were placed as extensions from the top and bottom helices in Figure 1a, the DNA origami rectangles (using staple strands "M$\underline{Y}$", Figures 2c and S3) tend to bend to form size-limited 1D short DNA nanotubes (Figure 2d) rather than linear oligomerization. Indeed, we did not observe any oligomeric DNA origami shapes under AFM imaging. Instead, we observed two types of size-limited structures, rectangular DNA origami (yield <15%) and rod-like structures (yield >85%). AFM measurements showed that the length, width, and height of these rod-like structures are of ~100, ~35, and ~4 nm, respectively (Figure S18), corresponding to the same length, half of the width, and twice of the height of the rectangular structures, suggesting that they are double-layer rectangles (compressed nanotubes). We note that the AFM images alone are not sufficient to confirm the formation of tube shapes due to the compression and possible damage of the nanostructure with the exerted forces of AFM tips. In fact, by increasing the scanning force exerted on these rod-like structures, they were easily turned into planar thin origami pieces; some of them
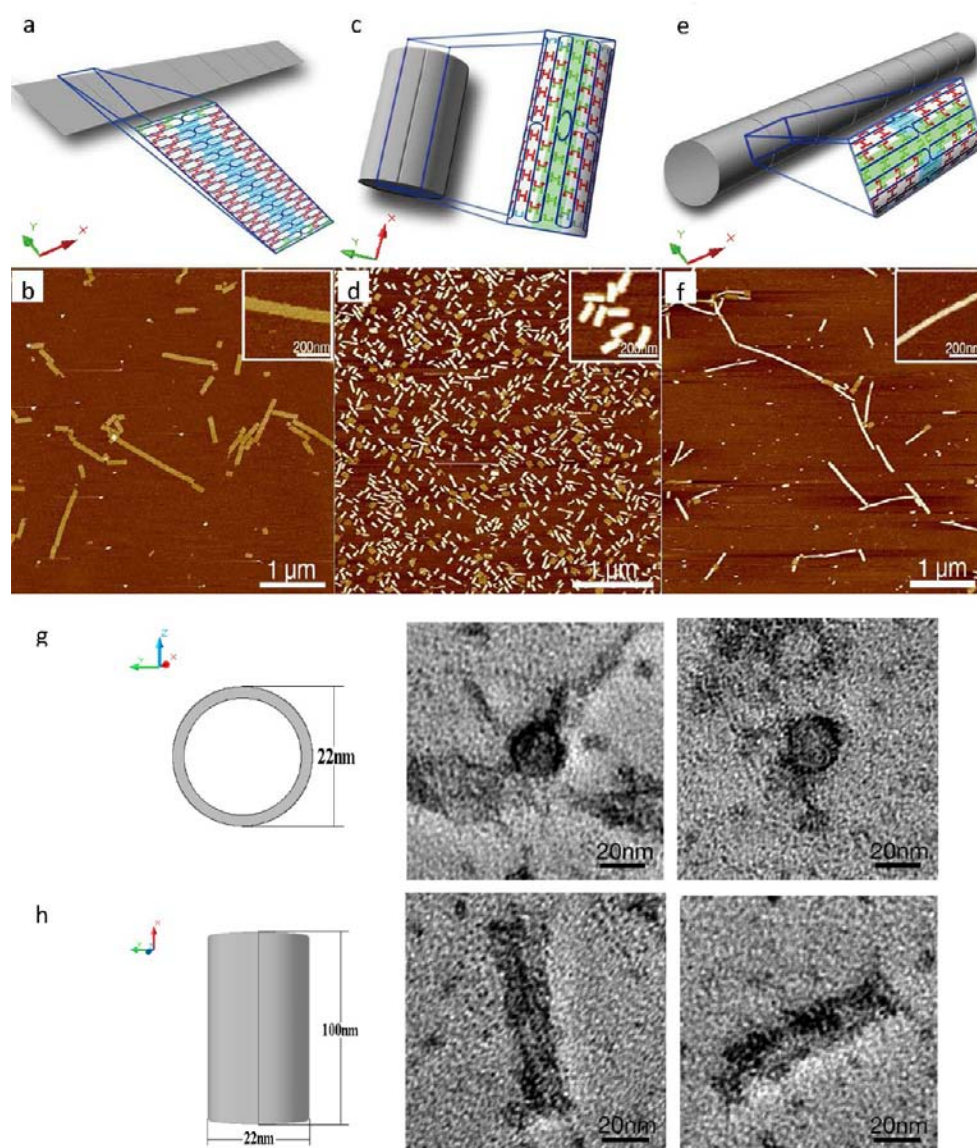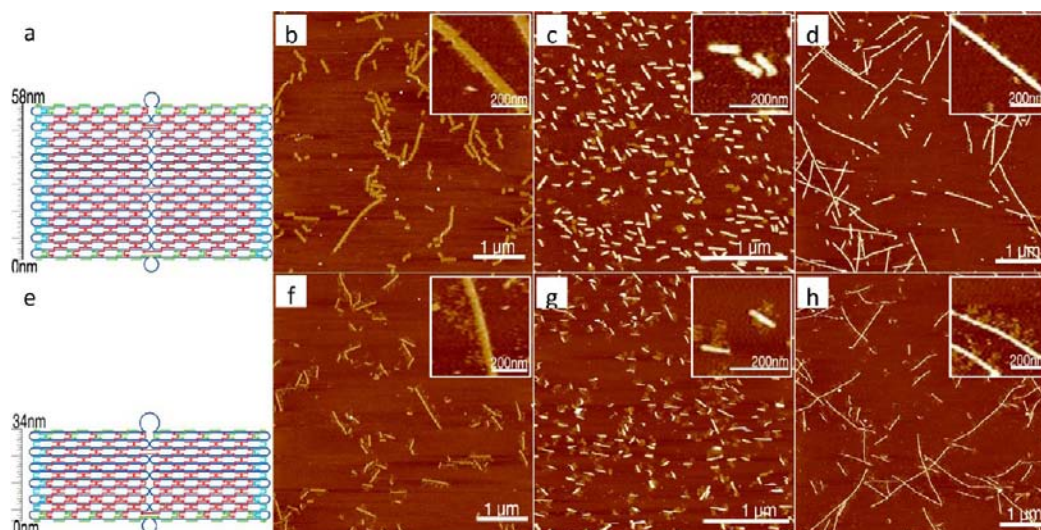
Figure 2. Schematic illustrations and AFM images for 1D higher-order DNA origami combinatorial structures. (a,b) DNA origami nanoribbons.(c,d) Short DNA origami nanotubes. (e,f) Long DNA origami nanotubes. (g) Top-view schematic diagram and TEM images; (h) Side-view schematic diagram and TEM images of short DNA origami nanotubes.

were even broken into smaller fragments (Figure S19). Transmission electron microscopy (TEM) provides direct evidence for the successful formation of the nanotube shape. We observed the presence of vertically aligned tube-like structures by TEM imaging, indicating that they are indeed nanotube structures with a uniform diameter of ~20 nm (Figure 2g,h). In addition, the length and the width of the short nanotubes are ~90 and ~20 nm, respectively, which is slightly different with those obtained by AFM. We suggest that origami is more flexible for bending orthogonal to the helices rather than in parallel with the helices. Therefore, the self-assembly behavior observed for rectangles with top/bottom was different from that with left/right sticky ends.

Formation of 1D Long DNA Nanotubes. We next modified all edge staples to establish sticky end connections at all four edges (using staple strands "M$\underline{X}$" and "M$\underline{Y}$", Figure 2e). After assembly of the origami, AFM imaging showed that the product is predominantly long nanotubes with ~4 nm in height, ~35 nm in width, and 0.5−3.5 μm in length (Figures 2f

and S16E), suggesting that rectangles bent upon themselves and assembled in the horizontal direction. Considering the diameter of 20 nm (as shown in TEM imaging of short nanotubes), the produced long nanotubes have aspect ratios of up to 175. Similar 1D nanotubes are also seen from the 2 h one-pot assembly (Figure S17B).

Diameter Control of DNA Nanotubes. This single-step strategy allows convenient control of width or diameter of combinatorial structures by varying the number of horizontal helices in the origami design (Figures S11−S13). By designing origami with 4 or 12 helices less from the top, we obtained narrower DNA nanoribbons with measured widths of ~61 and ~39 nm, respectively (Figure 3). Given that the width of each two helices equals ~6 nm in the rectangular origami, the theoretical widths of the modified origami with 4 or 12 rows removed are 58 and 34 nm, respectively, which coincides well with the experimental data. More importantly, very narrow nantubes with diameters of only 18 and 11 nm were also obtained by removing 8 and 12 helices without sacrificing yields

Figure 3. Width/diameter-control of the combinatorial structures. (a,e) Schematic illustrations of the rectangular DNA origami structures removing 4 and 12 helices. (b,f) AFM images of nanoribbons. (c,g) AFM images of short nanotubes. (d,h) AFM images of long nanotubes.
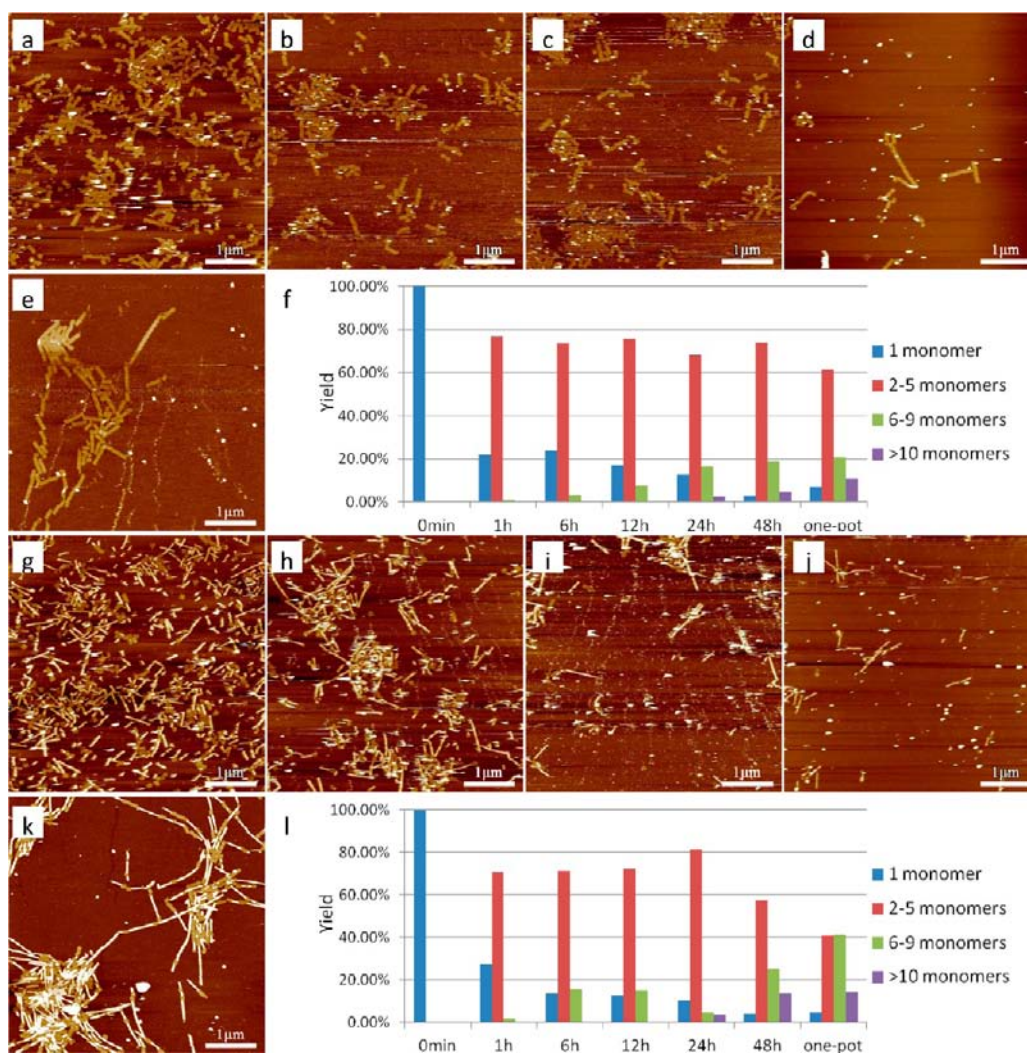

Figure 4. AFM images of time-dependent stepwise assembly of DNA nanoribbons (a−e) and long nanotubes (g−k) 1, 6, 12, 24, and 48 h, respectively. Yields of monomers, short oligomers (2−5 monomers) and long oligomers (6−9 monomers and >10 monomers) are counted and shown in (f) for nanoribbons and (l) for long nanotubes. Zero point was arbitrarily assigned to in a state of 100% monomers. The values one-pot methods are counted from images shown in Figure 2.
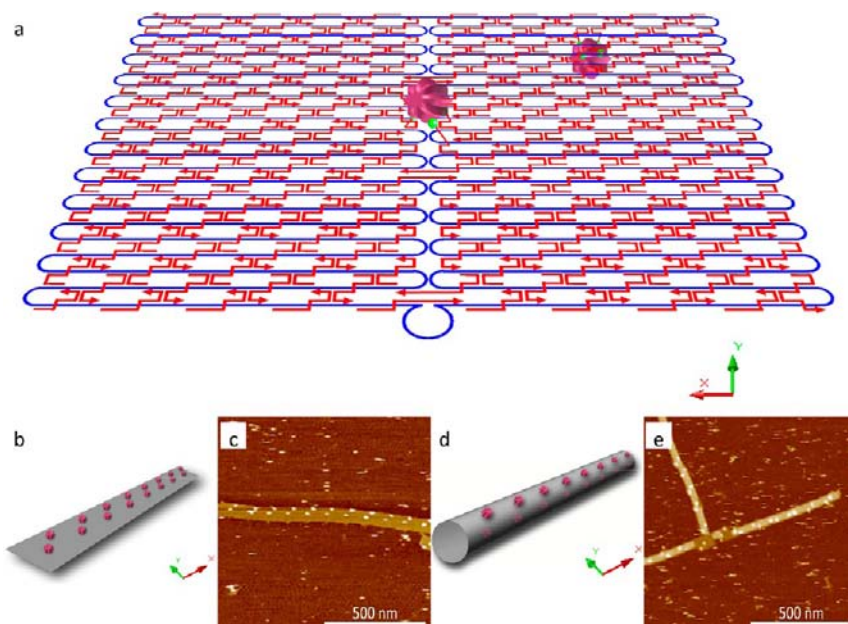
Figure 5. Directed assembly of protein arrays. (a) Schematic illustration of putting streptavidins on rectangular DNA origami. In this design, two streptavidins are anchored on the "up" and "down" sides of this DNA origami, respectively. (b,c) Streptavidin arrays on DNA origami nanoribbons. (d,e) Streptavidin arrays on long DNA origami nanotubes.
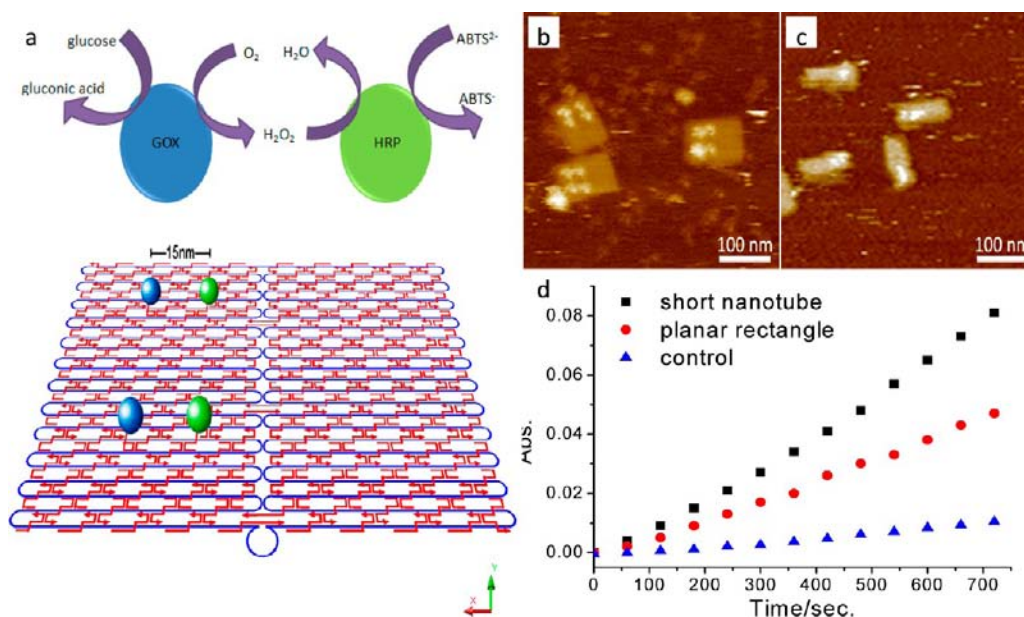
Figure 6. Enzyme cascade systems. (a) Schematic illustration of the bienzyme cascade of GOx and HRP on rectangular DNA origami. (b) AFM image of the enzyme cascade on rectangular DNA origami. (c) AFM image of the enzyme cascade in short DNA nanotubes. (d) Kinetics measurements of the enzyme cascade systems.

(Figure S21, Tables S1 and S2). Such ability to precisely control of the diameter of DNA nanotubes inherits from the superior recognition ability of DNA base-pairing and shows clear advantages over inorganic nanotubes.

Comparison with Stepwise Assembly. The above-mentioned DNA nanostructures can also be assembled in a conventional two-step method (Figures S4, S5, and S6 for nanoribbons, short nanotubes, and long nanotubes, respectively). To assemble DNA nanoribbons, rectangular origami pieces without sticky ends were first formed via a standard annealing process, after which 22 linker staples were added to perform horizontal assembly to obtain DNA nanoribbons

during a 2 day process (Figure S16B). Short and long DNA nanotubes can be similarly assembled in stepwise way (Figure S5, S6, S16D, and S16F). Furthermore, the time evolution of the stepwise assembly was monitored and compared with the one-pot method. We observed a clear trend of stepwise formation from monomer to short oligomers (2−5mer) and then to long oligomers (6−9mer and >10mer) with the increase of the assembly time, consistent with the expected multistep assembly process (Figure 4). DNA origami monomers are prone to form short oligomers in only 1 h. After that, the elongation of short oligomers seems to be much more difficult as this value has slow change during the 2 day

process. The yields of long oligomers also increased very slowly. As compared with the one-pot method, it takes much longer time to assemble long oligomers with the stepwise method. Noticeably, the ultimate yield of such a complex process is similar to that obtained with a one-pot assembly within 20 min, suggesting the high cooperativity in the latter case. Hence, while both the single- and two-step methods can result in desired nanostructures, the rapid assembly and high cooperativity in the single-step approach are clearly an advantage.

Addressable Protein Patterning. These DNA nanostructures are inherently addressable for anchoring biomolecules with nanoscale resolution and at the single-molecule level.[46] We first employed 1D nanoribbons as templates to direct the assembly of protein arrays (Figure 5b). On each rectangular origami monomer, two biotin molecules were anchored on the "up" and "down" sides, respectively, which was followed by streptavidin binding (Figure 5a). Figure 5c shows an AFM image of streptavidin-decorated DNA origami nanoribbons, from which two streptavidin molecules per origami are clearly visible with nearly 100% yield, and the interparticle distance is in good agreement with the theoretical prediction (Figure S22b). 1D nanotubes could also be used as templates for protein patterning. Since the diameter of the nanotubes is 22 nm, which is much larger than the size of streptavidin of 4−5 nm. Also, the two biotins are located at the two different surfaces of the rectangular nanostructure, it is expected that one is inside and that the other is outside of the folded nanotube (Figure 5d). Indeed, we find that two streptavidin proteins were assembled on each nanotube monomer with a yield of ∼100% (Figures 5e and S22d). This means that streptavidin can go into the nanotube and bind to biotin inside the nanotube even though the length of these nanotubes can be up to micrometers. This result inspired us that the as-prepared DNA nanotubes could be used as addressable nanocontainers for nanoparticles and biomolecules.

Enzyme Cascade Confined within the Short DNA Nanotube. By exploiting such unprecedented ability of precise positioning of biomolecules, we further constructed a nanoscale bioreactor by coupling two enzymes, GOx and HRP, in both the planar rectangular and short DNA origami nanotubes. GOx and HRP were positioned with a specific interenzyme distance (the distance between GOx and HRP) of 15 nm (Figure 6a), as confirmed with AFM imaging (Figure 6b,c). Their enzymatic coupling efficiency was quantitatively measured with the chromogenic reaction of the substrate of HRP, 2′2′-azino-bis[3-ethylbenzthiazoline-6-sulfonic-acid] ($ABTS^{2-}$). To simplify the analysis, we employed excess amounts of reactant glucose and reporter $ABTS^{2-}$. Hence, the efficiency of this enzyme cascade reaction on each specific DNA nanostructure is critically dependent on the diffusion of the biocatalytic intermediate, H_2O_2. As shown in Figure 6d, GOx and HRP positioned on both the rectangular nanostructure and within the short nanotube exhibited much higher efficiencies than the two enzymes freely dispersed in solution, an effect arising from high local concentration of the intermediate H_2O_2 due to the spatial control of the bienzyme pair.[47] Also, the enzyme cascade efficiency is dependent on the interenzyme distance (Figure S24), in coincidence with previously reported results.[48] Remarkably, the efficiency of this enzyme cascade within short nanotube (confined nanospace) was also significantly higher than that on the planar rectangle (semiconfined nanospace). Since the DNA rectangular nanostructure is only semiconfined, the intermediate H_2O_2 could diffuse in a

hemisphere. On the contrary, when both enzymes were confined within the DNA nanotubes, H_2O_2 could not diffuse out of the diffusion layer that was much thicker than the diameter of DNA nanotubes (20 nm), resulting in high coupling between the enzymes. We also carried out a control experiment with only HRP decorations on the rectangular DNA nanostructure. As shown in Figure S25, HRP also showed slightly higher activity when it was assembled on the DNA nanostructure as compared to free ones. Hence, the activity enhancement is a synergetic effect arising from both the stabilizing effect of the DNA nanostructure and the caging effect of the confined nanospace. While previous studies have well shown that catalytic efficiency becomes high when catalysts are encapsulated within inorganic nanomaterials,[10,11] our system provides a unique, unprecedented opportunity to site-specifically encapsulate enzymes with nanometer scale precision of spatial control, a property resembling highly organized and crowded environments of enzymes within cells.[49]

CONCLUSIONS

In summary, we have developed a reliable and facile single-step strategy for the construction of 1D DNA origami nanoribbons and nanotubes with high speed and cooperativity. The width/diameter control of these combinatorial nanostructures could be simply realized and precisely controlled. We expect that proper metallization[50] of these nanostructures may lead to novel nanoplasmonic materials with unprecedented properties. The DNA nanostructures are also useful as templates for protein patterning with sub-10 nm addressability, a unique property that is difficult to realize with inorganic nanomaterials. We demonstrated that these DNA nanostructures provide precisely controlled confined nanospace for site-specific positioning of proteins and efficient coupling of enzyme cascade, resulting in high-efficiency nanoscale bioreactors. It is also envisioned that they could be multiple labeling reagents carrying tunable numbers of tags as well as combined with DNA nanomotors to achieve controlled transportation and release *in vivo*.

ASSOCIATED CONTENT

Ⓢ Supporting Information

Detailed experimental procedures, detailed schematic illustrations, additional PAGE, absorption spectra, and AFM images. This information is available free of charge via the Internet at http://pubs.acs.org.

AUTHOR INFORMATION

Corresponding Author
fchh@sinap.ac.cn; liuhuajie@sinap.ac.cn
Author Contributions
‖These authors contributed equally.
Notes
The authors declare no competing financial interest.

ACKNOWLEDGMENTS

■ REFERENCES

(1) Lehn, J.-M. Science 2002, 295, 2400−2403.

(2) Ariga, K.; Hu, X.; Mandal, S.; Hill, J. P. Nanoscale 2010, 2, 198−214.

(3) Li, D.; Song, S.; Fan, C. Acc. Chem. Res. 2010, 43, 631−641.

(4) Saha, K.; Agasti, S. S.; Kim, C.; Li, X.; Rotello, V. M. Chem. Rev. 2012, 112, 2739−2779.

(5) Chen, P.; Pan, D.; Fan, C.; Chen, J.; Huang, K.; Wang, D.; Zhang, H.; Li, Y.; Feng, G.; Liang, P.; He, L.; Shi, Y. Nat. Nanotechnol. 2011, 6, 639−644.

(6) Baughman, R. H.; Zakhidov, A. A.; de Heer, W. A. Science 2002, 297, 787−792.

(7) Li, X.; Wang, X.; Zhang, L.; Lee, S.; Dai, H. Science 2008, 319, 1229−1232.

(8) Hu, W.; Peng, C.; Luo, W.; Lv, M.; Li, X.; Li, D.; Huang, Q.; Fan, C. ACS Nano 2010, 4, 4317−4323.

(9) He, S.; Song, B.; Li, D.; Zhu, C.; Qi, W.; Wen, Y.; Wang, L.; Song, S.; Fang, H.; Fan, C. Adv. Funct. Mater. 2010, 20, 453−459.

(10) Pan, X.; Fan, Z.; Chen, W.; Ding, Y.; Luo, H.; Bao, X. Nat. Mater. 2007, 6, 507−511.

(11) Fu, Q.; Li, W.; Yao, Y.; Liu, H.; Su, H.; Ma, D.; Gu, X.; Chen, L.; Wang, Z.; Zhang, H.; Wang, B.; Bao, X. Science 2010, 328, 1141−1144.

(12) Seeman, N. C. Nature 2003, 421, 427−431.

(13) Pinheiro, A. V.; Han, D.; Shih, W. M.; Yan, H. Nat. Nanotechnol. 2011, 6, 763−772.

(14) Steitz, T. A. Nat. Rev. Mol. Cell Biol. 2008, 9, 242−253.

(15) Rothemund, P. W. Nature 2006, 440, 297−302.

(16) Qian, L.; Wang, Y.; Zhang, Z.; Zhao, J.; Pan, D.; Zhang, Y.; Liu, Q.; Fan, C.; Hu, J.; He, L. Chin. Sci. Bull. 2006, 51, 2973−2976.

(17) Li, J.; Pei, H.; Zhu, B.; Liang, L.; Wei, M.; He, Y.; Chen, N.; Li, D.; Huang, Q.; Fan, C. ACS Nano 2011, 5, 8783−8789.

(18) Pei, H.; Lu, N.; Wen, Y.; Song, S.; Liu, Y.; Yan, H.; Fan, C. Adv. Mater. 2010, 22, 4754−4758.

(19) Zhang, Z.; Wang, Y.; Fan, C.; Li, C.; Li, Y.; Qian, L.; Fu, Y.; Shi, Y.; Hu, J.; He, L. Adv. Mater. 2010, 22, 2672−2675.

(20) Pei, H.; Liang, L.; Yao, G.; Li, J.; Huang, Q.; Fan, C. Angew. Chem., Int. Ed. 2012, 51, 9020−9024.

(21) Andersen, E. S.; Dong, M.; Nielsen, M. M.; Jahn, K.; Subramani, R.; Mamdouh, W.; Golas, M. M.; Sander, B.; Stark, H.; Oliveira, C. L.; Pedersen, J. S.; Birkedal, V.; Besenbacher, F.; Gothelf, K. V.; Kjems, J. Nature 2009, 459, 73−6.

(22) Kallenbach, N. R.; Ma, R.; Seeman, N. C. Nature 1983, 305, 829−831.

(23) Winfree, E.; Liu, F.; Wenzler, L. A.; Seeman, N. C. Nature 1998, 394, 539−44.

(24) Gothelf, K. V.; LaBean, T. H. Org. Biomol. Chem. 2005, 3, 4023−4037.

(25) He, Y.; Ye, T.; Su, M.; Zhang, C.; Ribbe, A. E.; Jiang, W.; Mao, C. Nature 2008, 452, 198−201.

(26) Ke, Y.; Lindsay, S.; Chang, Y.; Liu, Y.; Yan, H. Science 2008, 319, 180−3.

(27) Douglas, S.; Dietz, H.; Liedl, T.; Hogberg, B.; Graf, F.; Shih, W. Nature 2009, 459, 414−418.

(28) Jungmann, R.; Steinhauer, C.; Scheible, M.; Kuzyk, A.; Tinnefeld, P.; Simmel, F. C. Nano Lett. 2010, 10, 4756−4761.

(29) Kim, K. N.; Sarveswaran, K.; Mark, L.; Lieberman, M. Soft Matter 2011, 7, 4636−4643.

(30) Wilner, O. I.; Orbach, R.; Henning, A.; Teller, C.; Yehezkeli, O.; Mertig, M.; Harries, D.; Willner, I. Nat. Commun. 2011, 2, 540.

(31) Yan, H.; Park, S. H.; Finkelstein, G.; Reif, J. H.; LaBean, T. H. Science 2003, 301, 1882−4.

(32) Lo, P. K.; Karam, P.; Aldaye, F. A.; McLaughlin, C. K.; Hamblin, G. D.; Cosa, G.; Sleiman, H. F. Nat. Chem. 2010, 2, 319−328.

(33) Nykypanchuk, D.; Maye, M. M.; Lelie, D.; Gang, O. Nature 2008, 451, 549−552.

(34) Park, S. Y.; Lytton-Jean, A. K. R.; Lee, B.; Weigand, S.; Schatz, G. C.; Mirkin, C. A. Nature 2008, 451, 553−556.

(35) Cheng, W.; Campolongo, M. J.; Cha, J. J.; Tan, S. J.; Umbach, C. C.; Muller, D. A.; Luo, D. Nat. Mater. 2009, 8, 519−525.

(36) Han, D.; Pal, S.; Nangreave, J.; Deng, Z.; Liu, Y.; Yan, H. Science 2011, 332, 342−346.

(37) Han, D.; Pal, S.; Liu, Y.; Yan, H. Nat. Nanotechnol. 2010, 5, 712−717.

(38) Kuzyk, A.; Schreiber, R.; Fan, Z.; Pardatscher, G.; Roller, E.-M.; Hogele, A.; Simmel, F. C.; Govorov, A. O.; Liedl, T. Nature 2012, 483, 311−314.

(39) Endo, M.; Sugita, T.; Katsuda, Y.; Hidaka, K.; Sugiyama, H. Chem.—Eur. J. 2010, 16, 5362−5368.

(40) Jungmann, R.; Scheible, M.; Kuzyk, A.; Pardatscher, G.; Carlos, E. C.; Simmel, F. C. Nanotechnology 2011, 22, 275301.

(41) Zhao, Z.; Yan, H.; Liu, Y. Angew. Chem., Int. Ed. 2010, 49, 1414−1417.

(42) Endo, M.; Sugita, T.; Rajendran, A.; Katsuda, Y.; Emura, T.; Hidaka, K.; Sugiyama, H. Chem. Commun. 2011, 47, 3213−3215.

(43) Rajendran, A.; Endo, M.; Katsuda, Y.; Hidaka, K.; Sugiyama, H. ACS Nano 2011, 5, 665−671.

(44) Dietz, H.; Douglas, S. M.; Shih, W. M. Science 2009, 325, 725−730.

(45) Woo, S.; Rothemund, P. W. K. Nat. Chem. 2011, 3, 620−627.

(46) Numajiri, K.; Yamazaki, T.; Kimura, M.; Kuzuya, A.; Komiyama, M. J. Am. Chem. Soc. 2010, 132, 9937−9939.

(47) Wilner, O. I.; Weizmann, Y.; Gill, R.; Lioubashevski, O.; Freeman, R.; Willner, I. Nat. Nanotechnol. 2009, 4, 249−254.

(48) Fu, J.; Liu, M.; Liu, Y.; Woodbury, N. W.; Yan, H. J. Am. Chem. Soc. 2012, 134, 5516−5519.

(49) Ringe, D.; Petsko, G. A. Science 2008, 320, 1428−1429.

(50) Liu, J.; Geng, Y.; Pound, E.; Gyawali, S.; Ashton, J. R.; Hickey, J.; Woolley, A. T.; Harb, J. N. ACS Nano 2011, 5, 2240−2247.